International Journal of
Molecular Sciences

MDPI

Article

Urea-Peptide Hybrids as VEGF-A_{165}/NRP-1 Complex Inhibitors with Improved Receptor Affinity and Biological Properties

Anna K. Puszko [1,*,†], Piotr Sosnowski [2,†], Rachel Rignault-Bricard [3,4], Olivier Hermine [3,4], Gérard Hopfgartner [2], Karolina Pułka-Ziach [1], Yves Lepelletier [3,4] and Aleksandra Misicka [1,5,*]

1 Faculty of Chemistry, University of Warsaw, Pasteura 1, 02-093 Warsaw, Poland; karola@chem.uw.edu.pl
2 Department of Inorganic and Analytical Chemistry, University of Geneva, 24 Quai Ernest Ansermet, CH-1211 Geneva, Switzerland; piotr.sosnowski@unige.ch (P.S.); gerard.hopfgartner@unige.ch (G.H.)
3 Imagine Institute, Université de Paris, 24 boulevard Montparnasse, 75015 Paris, France; rachel.rignault@parisdescartes.fr (R.R.-B.); ohermine@gmail.com (O.H.); y.lepelletier@gmail.com (Y.L.)
4 INSERM UMR 1163, Laboratory of Cellular and Molecular Basis of Normal Hematopoiesis and Hematological Disorders: Therapeutical Implications, 24 Boulevard Montparnasse, 75015 Paris, France
5 Department of Neuropeptides, Mossakowski Medical Research Centre, Polish Academy of Sciences, Pawinskiego 5, 02-106 Warsaw, Poland
* Correspondence: apuszko@chem.uw.edu.pl (A.K.P.); misicka@chem.uw.edu.pl (A.M.)
† A.K.P. and P.S. contributed equally to this work.

Abstract: Neuropilin-1 (NRP-1), the major co-receptor of vascular endothelial growth factor receptor-2 (VEGFR-2), may also independently act with VEGF-A_{165} to stimulate tumour growth and metastasis. Therefore, there is great interest in compounds that can block VEGF-A165/NRP-1 interaction. Peptidomimetic type inhibitors represent a promising strategy in the treatment of NRP-1-related disorders. Here, we present the synthesis, affinity, enzymatic stability, molecular modeling and in vitro binding evaluation of the branched urea–peptide hybrids, based on our previously reported Lys(*h*Arg)-Dab-Oic-Arg active sequence, where the Lys(*h*Arg) branching has been modified by introducing urea units to replace the peptide bond at various positions. One of the resulting hybrids increased the affinity of the compound for NRP-1 more than 10-fold, while simultaneously improving resistance for proteolytic stability in serum. In addition, ligand binding to NRP-1 induced rapid protein stock exocytotic trafficking to the plasma membrane in breast cancer cells. Examined properties characterize this compound as a good candidate for further development of $VEGF_{165}$/NRP-1 inhibitors.

Keywords: peptidomimetics; amide bond mimetic; neuropilin-1; VEGF-A_{165}; protein–ligand interaction

Citation: Puszko, A.K.; Sosnowski, P.; Rignault-Bricard, R.; Hermine, O.; Hopfgartner, G.; Pułka-Ziach, K.; Lepelletier, Y.; Misicka, A. Urea-Peptide Hybrids as VEGF-A_{165}/NRP-1 Complex Inhibitors with Improved Receptor Affinity and Biological Properties. *Int. J. Mol. Sci.* **2021**, *22*, 72. https://dx.doi.org/10.3390/ijms22010072

Received: 16 November 2020
Accepted: 19 December 2020
Published: 23 December 2020

1. Introduction

The most important member from the vascular endothelial growth factors (VEGFs) family is the VEGF-A_{165} isoform, which has been shown to play major roles in physiological and pathological angiogenesis [1,2]. It also affects vascular permeability through binding to type III tyrosine kinase receptors from the vascular endothelial growth factor receptors (VEGF-R) family: VEGF-R1 and VEGF-R2 [1–5]. Another significant receptor for VEGF-A_{165} is neuropilin-1 (NRP-1), expressed on endothelial cells and responsible for enhancing the VEGF-A_{165}/VEGF-R2 signaling as a co-receptor, thereby increasing endothelial cell proliferation and migration and promoting angiogenesis [6–9]. NRP-1 is a transmembrane glycoprotein without catalytic activity. Apart from a role in the formation of new blood vessels, it participates in many signaling pathways, such as regulation of neuronal guidance [10], modulation of the immune response [11,12] and cell migration and survival. Despite the lack of catalytic activity, NRP-1 is considered to be an independent mediator of tumor development and progression, since it is extensively overexpressed in many cancerous cells [13–16], which is associated with tumor progression, metastasis and poor clinical outcome [17–19]. Therefore, the search for compounds that will inhibit the

formation of the VEGF-A_{165}/NRP-1 complex (Figure 1) may contribute to the development of potential anti-cancer drugs in the future. On the other hand, induction of angiogenesis and thus activation of NRP-1 is a therapeutic hope due to its usefulness in diseases such as coronary artery disease, stroke and impaired wound healing [7,20,21]. Strategies of blocking VEGF-A_{165}/NRP-1 complex formation to modulate angiogenesis are currently extensively studied. Designed inhibitors include small molecules [22–29] and linear [30–46] and cyclic [47–50] peptides or peptidomimetics.

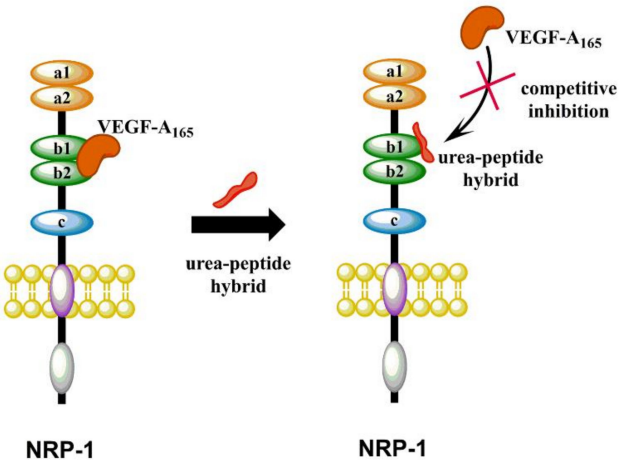

Figure 1. Schematic cartoon representing the VEGF-A_{165}/NRP-1 complex formation inhibited by synthesized urea–peptide hybrids.

Peptides are generally selective molecules that bind to specific cell surface receptors and are capable of initiating intracellular effects. Their specificity ensures safety, excellent tolerability and efficacy in therapy [51]. It has been proved that the binding pocket of NRP-1, b1-domain, requires the presence of C-terminal Arg/Lys-Xaa-Xbb-Arg/Lys motif in the ligands [2,35,36,52]. This absolute structural condition is called C-end rule (CendR) [35,36]. The C-terminal sequence of VEGF-A_{165} (CDKPPR) is responsible for growth factor interaction with NRP-1 and follows CendR [52–55]. CendR motif occurs in the sequences of many active peptides with proved affinity for NRP-1, e.g., A7R [30,32,34,56], tuftsin [31] and penetrating iRGD peptide [57]. Unfortunately, naturally occurring peptides have intrinsic flaws, such as poor chemical and physical stability, short circulating plasma half-lives, fast clearance and low membrane permeability [58,59]. Some of these drawbacks might be successfully resolved through modifications, such as the introduction of unnatural amino acids, amide bond mimetics, cyclisation (including stapling) and clipping of peptide sequences. As described recently in the literature, active pseudopeptides or compounds with peptide bond surrogates are particularly attractive; these include reduced peptide bonds [CH_2NH] [60,61], ester bonds in depsipeptides [62], thioamides [CSNH] [63–65], 1,2,3-triazoles (1,4 or 1,5-disubstituted) [66–68] and urea and thiourea bonds [69–72]. The amide bond surrogates maintain three-dimensional structures similar to those of natural peptides, but may possess different polarity, which could affect the formation of hydrogen bonds or acid-base interactions [73]. Most importantly, pseudopeptides are more resistant to the proteolytic degradation, due to the enzymes not recognizing properly the cleaving site.

We have recently developed short branched peptides with significant inhibitory effects on VEGF-A_{165}/NRP-1 complex formation [42,44]. The most promising among them have the Lys(*h*Arg)–Dab–Oic–Arg sequence, where the ε-amino group of Lys forms an amide bond with homoarginine (*h*Arg) carboxyl group [44]. To obtain more stable analogues, the side chain of the Lys residue in the first position was coupled with Arg urea moiety [45]. The resulting compound Lys(Arg^U)–Dab–Oic–Arg exhibited similar inhibitory activity compared to the parent sequence, but its enzymatic stability was significantly higher. In

the presented study, in order to further induce the enzymatic stability and activity of NRP-1 ligands, we designed compounds based on branched Lys(*h*Arg) fragment, which was modified using various urea units. Synthesis, inhibitory activity against the VEGF-A_{165}/NRP-1 complex, enzymatic stability, molecular modelling and in vitro analysis of the derivatives with introduced urea bonds are described. This work is the next step in structure–activity relationship (SAR) studies for ligand–NRP-1 interactions and the development of prospective drug candidates.

2. Results and Discussion

2.1. Design Strategy

Identifying sites for the hydrolysis of the compound by proteases is one of the steps for the rational design of peptidomimetics. It can indicate parts of the molecule that need chemical modifications to increase the biological stability of the compound. Our aim was to design enzymatically stable, short and branched peptidomimetics, based on our previously described Lys(*h*Arg)-Dab-Oic-Arg sequence, which exhibits highly competitive inhibition of NRP-1/VEGF-A_{165} complex formation [44]. Lys(*h*Arg) branching is crucial for obtaining high affinity to NRP-1 receptor, but undergoes enzymatic hydrolysis primarily. Considering that a urea moiety might enhance stability and provide additional hydrogen bond donor through an extra –NH– group, which may generate additional interactions sites with target, it could be considered as a beneficial peptide bond surrogate [74]. However, such a replacement might also affect a compound's inhibitory activity. Our previous studies showed that the substitution of Lys-ε-*h*Arg amide bond by urea group and replacement of *h*Arg with shorter Arg side chain made peptidomimetics more resistant to enzymatic cleavage, but it also affected the affinity for NRP-1. The inhibitory activity of the most potent Lys(*h*Arg)-Dab-Oic-Arg peptide (IC_{50} = 2.3 μM) [44] decreased about two-fold due to introduction of urea bond (IC_{50} = 5.5 μM) [45]. Lower inhibitory activity might be related to N-terminus branching elongation, as urea moiety changed the number of atoms in the chain, thereby suggesting further refinement of Lys(*h*Arg) part. The applied combination of building blocks provides the same branching length as present in the Lys(*h*Arg) fragment of parent sequence but modifies the position of individual residues and the location of the urea bond. Three different strategies were envisioned (Figure 2a) and the following sites were modified: between the carboxylic group of Lys (L1) and α-amino group of Dab in L2 (Figure 2b); between the carboxylic group of *h*Arg (L1′) and ε-amino group of Lys in L1 (Figure 2c); in both sites simultaneously (Figure 2d).

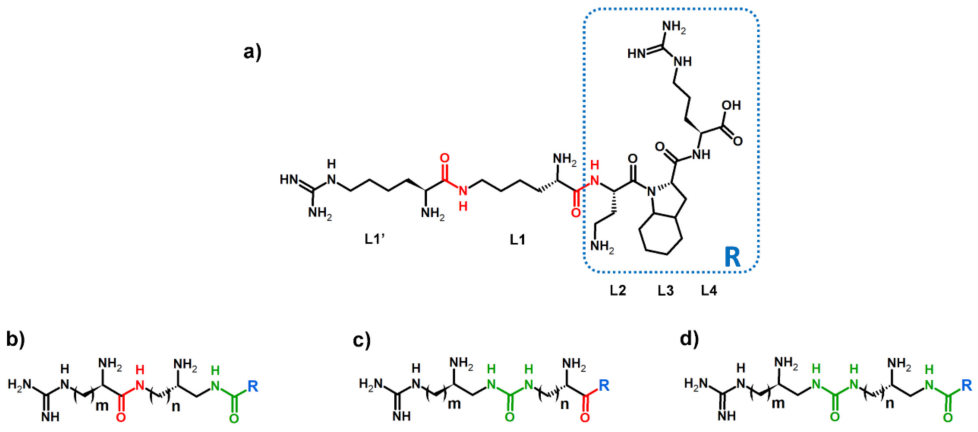

Figure 2. (**a**) Parent sequence with marked amide bonds (red) intended for modification. L denotes the position of the amino acid in the sequence. The general structure of urea–peptide hybrids branching in (**b**) compounds **1**, **2** and **3**; (**c**) compounds **4**, **5** and **6**; and (**d**) compounds **7**, **8** and **9** with urea bonds marked (green).

2.2. Synthesis

To introduce urea units into the peptidomimetic sequence, Boc-protected succinimidyl carbamate building blocks with side chain amino groups masked as azide groups or succinimidyl carbamate building blocks with α-amino groups masked as azide groups were used. The general synthesis of such activated building blocks is well described in the literature [75], and a simplified pathway with NMR data is presented in Supplementary Materials (Scheme S1, Figures S1–S5). The synthesis of urea–peptide hybrids was carried out following the Fmoc chemistry [76] using O-(1H-6-chlorobenzotriazole-1-yl)-1,1,3,3-tetramethyluronium hexafluorophosphate (HCTU) [77] as a coupling reagent and *N*,*N*-diisopropylethylamine (DIPEA) as a base. Active carbamate building block coupling and azide reduction were supported by microwave irradiation as previously described [45,75]. Guanidinylation reaction of side chain amino group in L1′ position was performed for 7 days using 3,5-dimethylpyrazole-1-carboxamidine nitrate (DMPCN) [78]. The synthesis pathway can be found in Scheme 1. The remaining compounds were synthesized in an analogous manner using sequence-appropriate building blocks and by carrying out, respectively, coupling and amine deprotection reactions for amino acids or coupling and azide reduction to amine for urea units. When Arg or *h*Arg residues were incorporated in L1′, the guanidinylation step was omitted. The structures of all obtained compounds were confirmed by HRMS and MS/MS fragmentation present in Supplementary Materials (Tables S1–S3, Figures S6–S15).

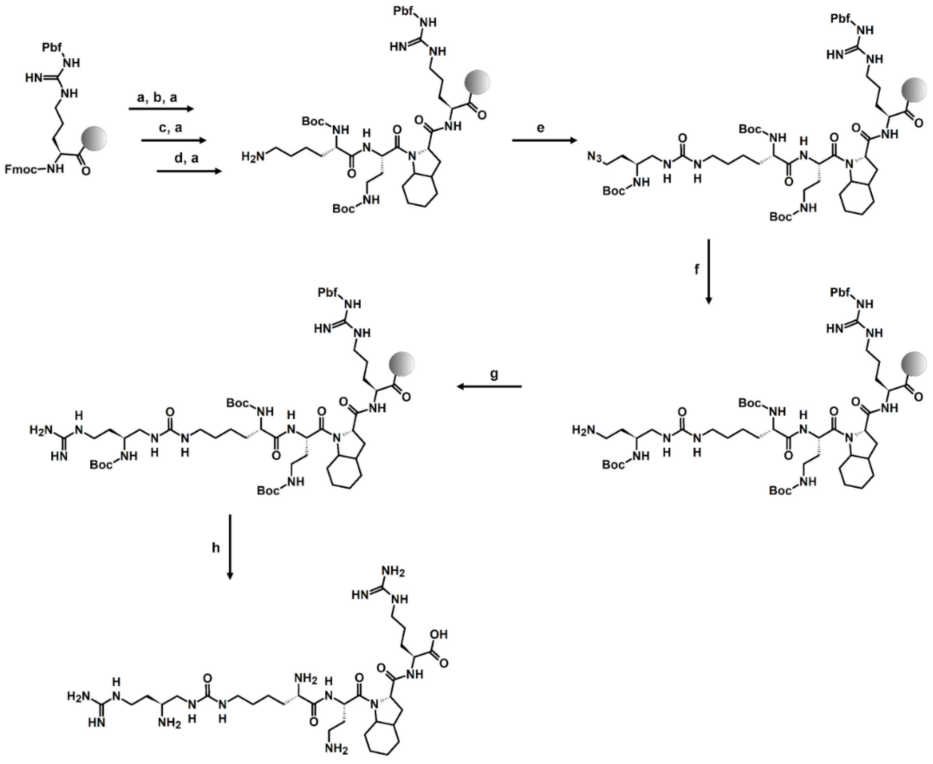

Scheme 1. The solid-phase peptide synthesis (SPPS) strategy on the example of urea–peptide hybrid **4**: (**a**) 20% piperidine in DMF; 20 min; (**b**) 2 eq Fmoc-Oic-OH, 2 eq HCTU, 5 eq DIPEA, 90 min; (**c**) 2 eq Fmoc-Dab(Boc)-OH, 2 eq HCTU, 5 eq DIPEA, 90 min; (**d**) 2 eq Boc-Lys(Fmoc)-OH, 2 eq HCTU, 5 eq DIPEA, 90 min; (**e**) 1.5 eq Boc-Dab(N_3) BB, 3 eq DIPEA, 50 W, 60 °C, 2 × 15 min; (**f**) 10 eq 1 M PMe_3/THF, 7:3 1,4-dioxane:H_2O, 50 W, 60 °C, 2 × 30 min; (**g**) 5 eq DMPCN, 19.5 eq DIPEA, 7 days; (**h**) 95:2.5:2.5 TFA:H_2O:TIS, 3 h.

2.3. Receptor Binding Studies

Inhibitory activity of urea–peptide hybrids against VEGF-A_{165}/NRP-1 complex formation was assessed with a screening ELISA-like assay. NRP-1 was immobilized on

microplate wells by simple adsorption and urea–peptide hybrids competed for NRP-1 with biotinylated VEGF-A_{165} (bt-VEGF-A_{165}). The amount of receptor bound bt-VEGF-A_{165} was visualized by its interaction with the streptavidin–horseradish peroxidase conjugate (strep-HRP) and the chemiluminescent substrate. The first analyzed group of compounds were analogues **1**–**3** with the urea bond between L1 and L2. Obtained results show that this modification does not affect binding of hybrids to the receptor significantly (IC_{50} = 1.2–2.2 μM), compared to the parent peptide (IC_{50} = 2.3 μM) (Table 1). The best hybrid in this group was compound **3**, which had Lys^U (gDab) branching (where "g" corresponds to guanidinium group), but its IC_{50} value decreased only 2-fold. Therefore, we assume that no additional interactions between urea bond and the surface of the protein occurred. Similarly, no significant change of affinity was observed for third group of compounds with two urea bonds in branching. IC_{50} values for hybrids **7**–**9** were between 1.8–2.1 μM. The most interesting group proved to be urea–peptide hybrids **4**–**6** with modification between L1 and L1′, where inhibitory activity increased 5 to 12-fold. Overall, the most promising among all analogues is hybrid **6** with IC_{50} = 0.19 μM. Our previous molecular modelling studies of branched peptides, with structures similar to the parent sequence, showed that the branching might lay over the receptor surface and interact with protein via the guanidinium group and/or α-amino group of *h*Arg [42]. However, the lack of the crystal structure of the branched peptide/receptor complex significantly hinders SAR studies and prediction of the effects of modifications to ligand–receptor interactions. In the case of urea–peptide hybrids, the urea bond might be capable of forming additional hydrogen bonds with protein residues on the surface of NRP-1. The affinity of compounds may conceivably be affected by the colocation of the urea bond and the free amino group of *h*Arg in the branching. In addition, for compounds **4**–**6**, we can observe that decreasing the distance between the free amino group in the main chain and the urea bond in the branching has a positive effect on compounds' affinity for NRP-1.

Binding selectivity is one of the crucial requirements on the path toward development of a non-hazardous therapeutics, as nonspecific binding generates a risk of causing unwanted side effects. However, absolute selectivity for a single protein is most often unreachable. An appropriate selectivity profile can lead to better drug properties by targeting multiple proteins, eventually leading to further benefits [79,80].

The most potent urea–peptide hybrid, **6**, was subjected to the analysis of selectivity to angiogenesis associated receptors, NRP-2, VEGF-R1 and VEGF-R2, which form a complex with VEGF-A_{165}. Amino acid sequence homology for primary structures of NRP-1 and NRP-2 is 44% [81,82]. Structural studies have shown that both receptors bind VEGF-A_{165} using a conserved binding pocket core, formed by the b1 subdomain loops [83]. VEGF-A_{165} interacts also with VEGF-R1 and R2 receptors by different fragments encoded by exons 1–5 [84,85]. Affinity studies were done using modified ELISA-like assay, performed in the same manner as affinity tests for NRP-1 after optimization of method for individual protein. Obtained results show that urea–peptide hybrid **6** exhibits high inhibitory activity with the IC_{50} = 0.48 μM against VEGF-A_{165}/NRP-2 complex formation (Table 2). However, this value is more than two times higher compared to VEGF-A_{165}/NRP-1 complex inhibition. At the same time, our data suggest no affinity for both VEGF-Rs.

Table 1. The general structure and VEGF-A_{165}/NRP-1 complex inhibitory effect of X(Z)-Dab-Oic-Arg branched urea–peptide hybrids. Urea bonds are marked in green.

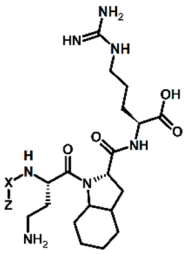

X(Z)-Dab-Oic-Arg

Compound	X(Z) Branching	X(Z) Branching Structure	IC_{50} [μM] [1]
PP	Lys(*h*Arg)	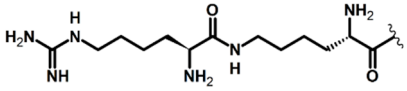	2.3 [2]
1	Dab^{U}(*h*Arg)	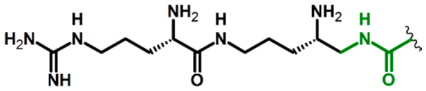	1.8 [3]
2	Orn^{U}(Arg)	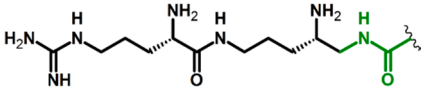	2.1 [4]
3	Lys^{U}(gDab)	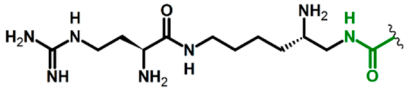	1.2 [5]
4	Lys($gDab^{U}$)	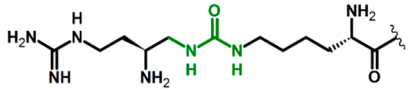	0.49 [6]
5	Orn(Arg^{U})	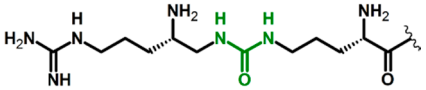	0.36 [7]
6	Dab(*h*Arg^{U})	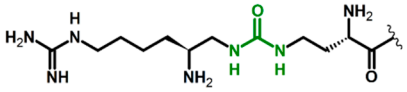	0.19 [8]
7	Dap^{U}(Arg^{U})	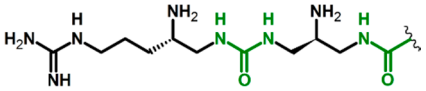	2.1 [9]
8	Dab^{U}($gDab^{U}$)	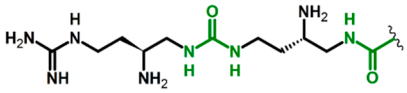	2.1 [10]
9	Orn^{U}($gDap^{U}$)	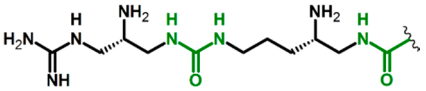	1.8 [11]

[1] R^2 ranged between 0.992 and 0.999. [2] Data already published [44]. [3] $logIC_{50}$ = −5.75 ± 0.03; [4] $logIC_{50}$ = −5.67 ± 0.01; [5] $logIC_{50}$ = −5.93 ± 0.03; [6] $logIC_{50}$ = −6.306 ± 0.024; [7] $logIC_{50}$ = −6.448 ± 0.031; [8] $logIC_{50}$ = −6.726 ± 0.028; [9] $logIC_{50}$ = −5.69 ± 0.02; [10] $logIC_{50}$ = −5.69 ± 0.03; [11] $logIC_{50}$ = −5.75 ± 0.03; compounds were tested in the concentration range 1–50 μM (compounds **1**–**3** and **7**–**9**) or 0.05–50 μM (compounds **4**–**6**). PP = parent peptide.

Table 2. Urea–peptide hybrid **6**'s inhibitory effect on VEGF-A_{165}/receptor complex formation.

Compound	Sequence	IC_{50} [μM]			
		NRP-1	NRP-2	VEGF-R1	VEGF-R2
6	H-Dab(*h*Arg^{U})Dab-Oic-Arg-OH	0.19	0.48 [1]	no affinity	no affinity

[1] logIC50 = −6.323 ± 0.043; R2 = 0.984; compound was tested in the concentration range 0.1–10 μM.

2.4. 2D NMR and Computational Study

2D NMR spectra were recorded to get an insight in to the structure of parent peptide and urea–peptide hybrid **6** in solution. Both compounds were dissolved in DPBS buffer with 10% addition of D_2O. Signals were assigned based on TOCSY, COSY and HSQC spectra (Figures S46–S50 and S52–S56). The analysis of ROESY spectra (Figure 3) indicated that both compounds exhibited very similar patterns of NOE connectivities. Most of ROESY signals overlapped perfectly well with the correlations observed at TOCSY (Figures S51 and S57); therefore, they reflected interaction only within one residue. For both compounds, we observed strong NOEs between sequential α-CH/NHpep protons and weak NOEs between some NHpep and CH_2 protons of neighboring amino acid residues in the branching (Figure 2). Any medium-range NOEs were not detected. All these observations indicated that parent peptide and hybrid **6** adopted quite similar extended and unstable conformations in solution [86]. It is also interesting to mention that NOE connectivity between protons of urea moiety in hybrid **6** was observed (Figure 3b), which may suggest trans/trans conformation of this urea group. NMR studies of the structure of the parent peptide and hybrid **6** in solution did not provide any explanation about differences in inhibitory activity against VEGF-A_{165}/NRP-1 complex formation.

In order to identify possible biding sites of parent peptide Lys (*h*Arg)Dab-Oic-Arg and urea–peptide hybrid **6**, we prepared complexes of both compounds with NRP-1 receptor and performed molecular dynamics simulations. Using the available 2ORZ crystallographic structure [33], where the C-terminal Arg residue of short peptide tuftsin is present in binding pocket of NRP-1, we superimposed both compounds' Arg residue on its counterpart in tuftsin. The remaining chain was set to extend outside of the protein, after which system was minimized and equilibrated. From this point, simulations were run independently in six repetitions for 200 ns each. Detailed information with graphs presenting evolution of the distance in time can be found in Supplementary Materials (Figures S58–S71). Many short-lived contacts could be observed; thus, it is impossible to indicate a single binding pose for in silico tested molecules, but the prevalence of selected interactions may explain the hybrid **6** increase of affinity. By comparing the simulation outcome for both molecules, we can observe a similar behavior of Arg residue in NRP-1 binding pocket to previously described results [41,42].

A summary of the observed interactions of both molecules in each run can be found in Supplementary Materials (Figure S72). A visual representation of binding poses is presented in Figure 4 with snapshots extracted from simulations. The most notable difference is in interactions of *h*Arg free amino group and urea moiety. In majorly present binding pose 1 (BP-1) both molecules could be described as "spread", similar to their 2D drawing. For the parent peptide, the guanidinium group of *h*Arg interacts with Glu319 and Glu324. N-terminal amine interacts through hydrogen bonding with Asp320, and other positively charged groups are directed outside of the protein (Figure 4). In the case of hybrid **6**, the urea moiety forms hydrogen bonds with Glu319 and "wraps" the molecule around this region, as at the same time interactions between free amino groups of *h*Arg^{U} with Glu319 and Dab (L1) with Glu319 or Asp320 are also observed. The guanidinium group of *h*Arg^{U} either forms interactions with nearby Glu324 or is exposed to solvent (Figure 4).

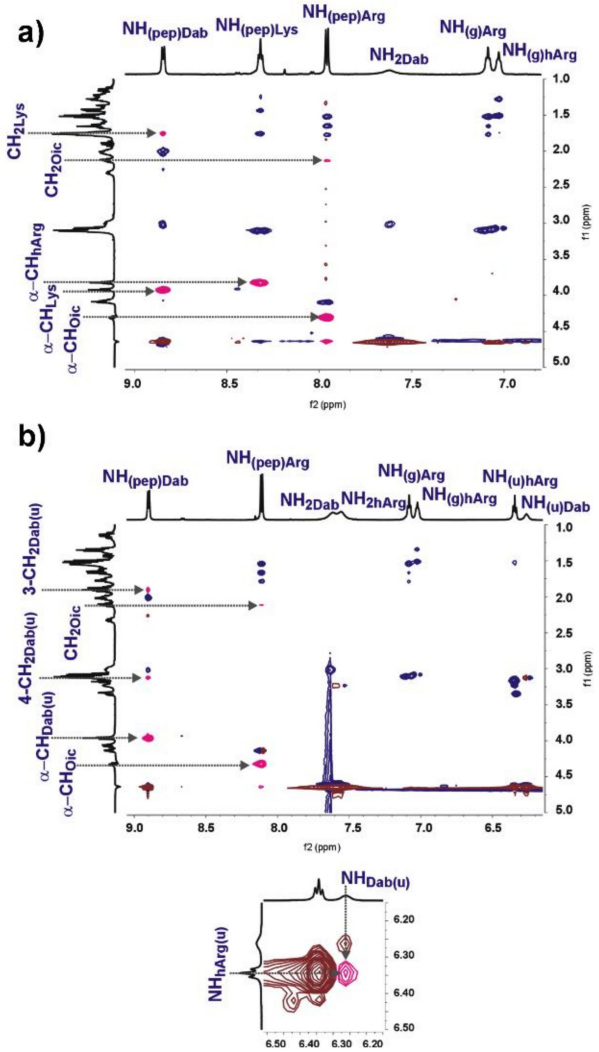

Figure 3. Part of NH/aliphatic region of ROESY spectra: NOEs between protons of different residues are marked with pink; (**a**) parent peptide; (**b**) hybrid **6** and NOE of NH/NH urea protons.

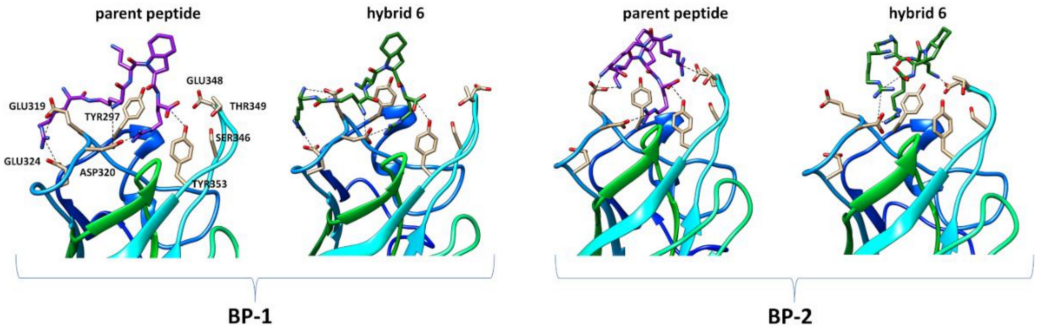

Figure 4. Molecular dynamics snapshots representing examples of binding poses between NRP-1 protein residues (PDB 2ORZ) and ligand functional groups for parent peptide and hybrid **6**.

In the much less frequent binding pose 2 (BP-2), the molecule is "twisted" in a manner such that the guanidinium group of *h*Arg or *h*Arg^{U} moiety is reaching the Glu348 (parent peptide) or Asp320 (hybrid **6**) while also forming the intra molecular interactions between carboxyl group of C-terminal Arg. This also promotes the formation of hydrogen bond between free amino group of Dab side chain and Glu319 (parent peptide) or Glu348 (hybrid

6). BP-2 was significantly present in 2 out of 6 simulations for parent peptide (*h*Arg-Glu348 contact for more than 50% simulation time) and 1 out of 6 simulations for hybrid **6** (*h*Arg^{U}-Arg contact for more than 50% simulation time).

2.5. In Vitro Enzymatic Stability

Rapid renal clearance and enzymatic degradation are classified as most important disadvantages of peptides as drugs. Covalent linkage to plasma proteins or chemical modifications, including amide bond modifications, might improve their half-lives [87]. We performed proteolytic stability studies in human blood serum to investigate whether the introduction of urea bonds affected the half-lives of compounds from each of synthesized group of hybrids. Compounds **3**, **6** and **7** were incubated with human serum at 37 °C. Samples were taken at different time intervals and analyzed using LC-SWATH-MS [88–90]. Identified cleavage sites were compared with the degradation of the parent peptide, which exhibited a half-life of 8 h. Hybrids **6** and **7** were stable toward enzymatic degradation, with 50% of each compound still being intact after 96 h (Figure 5). These analogues exhibit improved stability compared to the parent Lys (*h*Arg)-Dab-Oic-Arg sequence. In the case of hybrid **3**, degradation was significantly faster, and after 24 h only ~25% of initial substrate concentration remained in the sample. However, it was still more stable compared to the parent peptide. Overall, it can be concluded that the substitution of an amide bond with a urea bond has a positive effect on the proteolytic stability of the examined inhibitors.

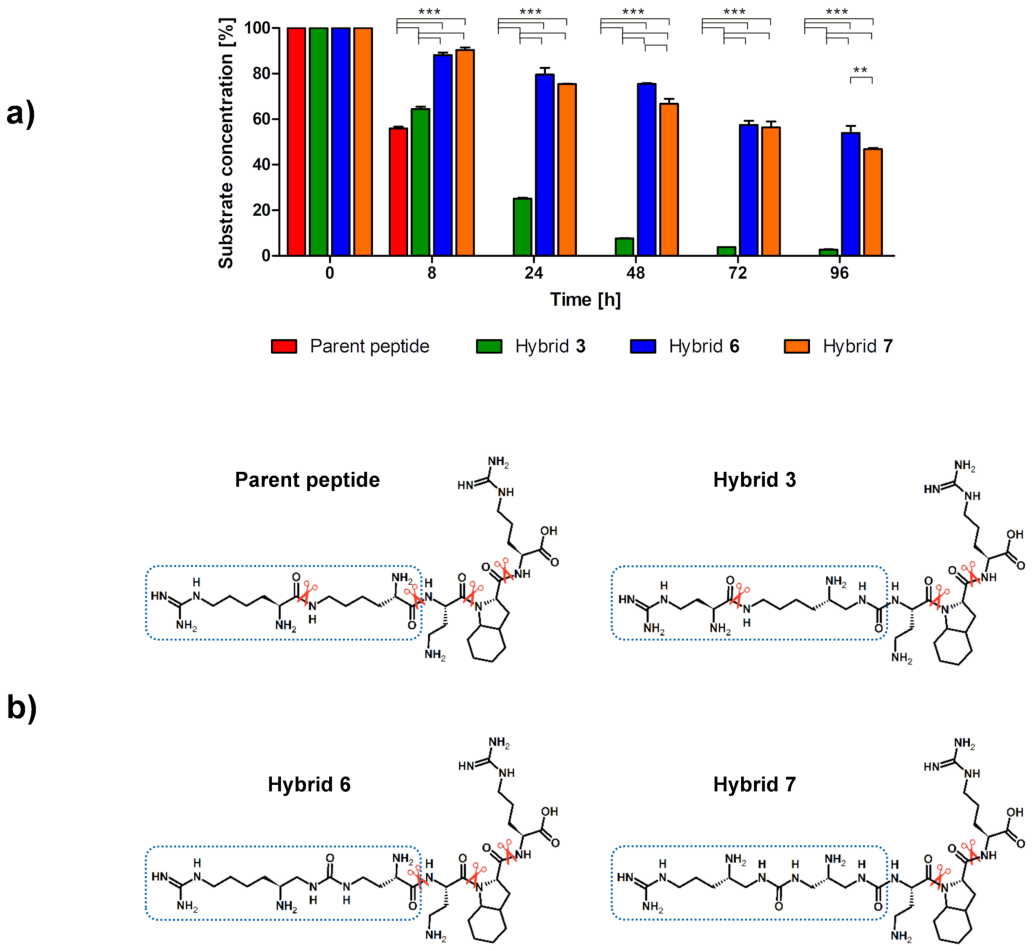

Figure 5. (**a**) Comparison of the in vitro metabolic stability of parent peptide and its urea–peptide hybrids **3**, **6** and **7**. Results are presented as the means ± SEMs of three independent experiments on LCMS (N = 3). In order to show significant differences in the concentration of intact substrate at each time interval depending on the sequence of the hybrid, a two-way ANOVA with Bonferroni's post-tests was done (** $p < 0.01$, *** $p < 0.001$). (**b**) Potential bonds cleaved by enzymes (scissors show identified proteases cleavage sites).

Analysis of the metabolites of urea–peptide hybrids by LC-MS, predicted by their theoretical masses, shows that urea bonds remained intact within the monitored time of the experiment (Tables S5–S8, Figures S17–S44). An example is the Dab-Oic-Arg (L2-L3-L4) metabolite, which is easily detected in the degradation of the parent peptide and hybrid **6**, but non-existent for hybrid **3** and **7**, where the peptide bond of AA-Dab (L1–L2) was substituted with its urea analogue. The results suggest that the bond between the side chain of the unit in L1 and L1′, which lengthens the branching, may play a significant role not only in the interaction with the receptor, but also in the stability of the branched compounds. Modification of this bond to obtain increase in enzymatic stability in serum was therefore justified.

2.6. Binding Assays on Cells

One of the methods applied for the detection of a compound, considering biological assays on living cells, is the application of a fluorescently tagged analogue for flow cytometry analysis. In order to carry out this experiment, we synthesized compound **10**, which is a hybrid of **6** labeled with 5/6-carboxyfluorescein (5/6-FAM) at N-terminus (5/6-FAM-Dab(*h*Arg^{U})-Dab-Oic-Arg). This molecule was first used to examine inhibitory activity of tagged hybrid against VEGF-A$_{165}$/NRP-1 complex formation using ELISA-like assay. The results show a significant increase of IC_{50} after labeling (IC_{50} = 4.04 μM) compared to unmodified compound (IC_{50} = 0.19 μM), but it must be noted that the 5/6-FAM tag may influence peptide affinity for NRP-1, e.g., due to its size. The IC_{50} value should be sufficient to prove compound interaction with NRP-1 (Table S4 in Supplementary Materials).

VEGF-A$_{165}$ binds to cell-surface NRP-1 on endothelial cells, effectively reducing surface levels of this receptor, promoting complex internalization and possibly inducing biological effects [91]. Based on this mechanism, peptide carriers for selective drug delivery, such as iRGD peptides, have been recently disclosed [57]. The iRGDs are used to selectively address potential therapeutic agents, e.g., doxorubicin or siRNAs inside malignant cells. We tested our tagged urea–peptide hybrid's ability to bind human NRP-1-positive breast cancer cells (MDA-MB-231), which expressed large amount of NRP-1 at the cell surface (Figure 6a). A broad range of concentrations between 0 to 100 μg/mL of compound **10** was used to show its binding capacity on cells using fluorescence-activated cell sorting (FACS). As shown in Figure 6b, binding on cells was dose-dependent. To follow the impact of the ligation of this peptidomimetic on NRP-1 expression, we verified whether hybrid **10** binding interferes with the antibody used to detect NRP-1. As we can observe in Figure 6c, the presence of compound **10** did not interfere with the NRP-1 detection (94 vs. 88 of median fluorescence intensity, respectively), allowing us the study of NRP-1 regulation in presence of these inhibitors. Finally, we performed co-staining (hybrid **10** and NRP-1 staining) to determine the ability (percentage) of NRP-1-positive MDA-MB-231 to bind compound **10**. All cells were able to bind our labeled hybrid and then all of these cells expressed NRP-1 (Figure 6d middle and right panels, respectively). In conclusion, we could follow the expression of NRP-1 by MDA-M-231 exposed to compound **10** using co-staining.

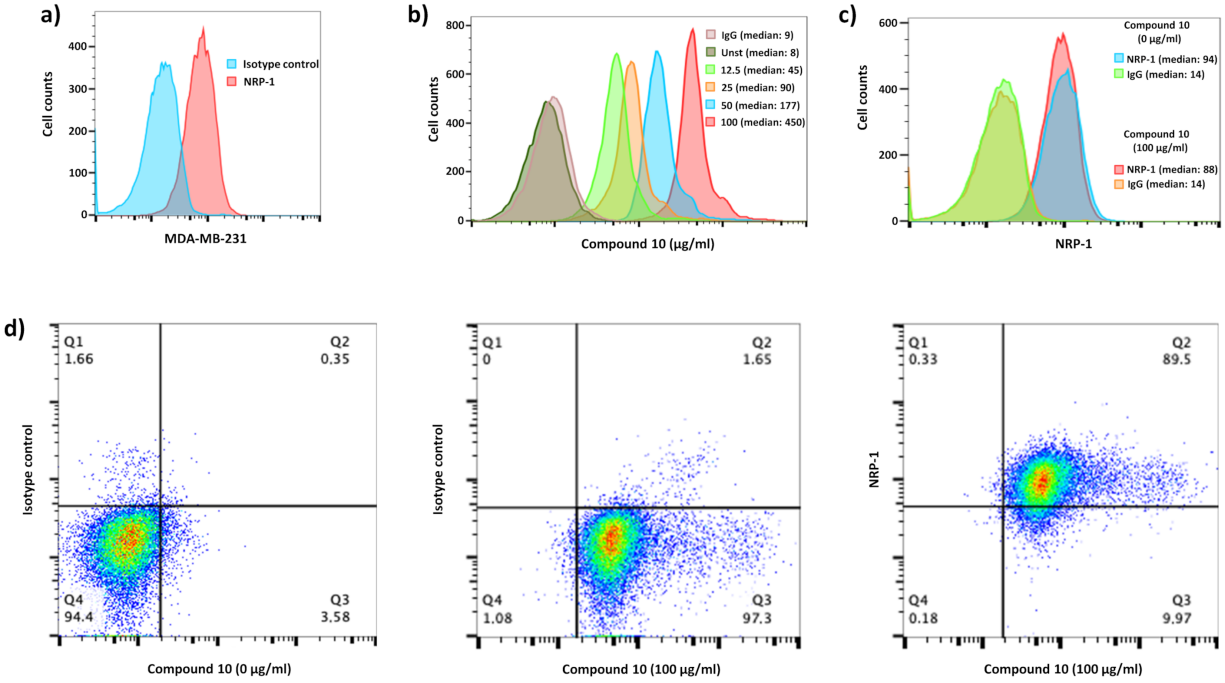

Figure 6. Compound **10** binds to NRP-1-positive MDA-MB-231 breast cancer cells. (**a**) Histogram shows NRP-1 level expression (red) compared to irrelevant control IgG staining (blue) on MDA-MB-231. (**b**) 5/6-FAM coupled with hybrid **6** (compound **10**) was used at 100 (red), 50 (blue), 25 (orange) and 12.5 (green) µg/mL to follow its positive binding on MDA-MB-231 compared to unstained (dark green) and FITC-irrelevant IgG (pink) as controls. Median fluorescence intensity is shown for each staining. (**c**) The histogram shows the uncompetitive and steric access for the NRP-1 staining in the presence (blue) of compound **10** compared to its absence (red). Both NRP-1 stainings are compared to irrelevant control IgG staining (green and orange respectively). Median fluorescence intensity is shown for each staining. (**d**) Dot plots show cells expressing NRP-1, which bound fluorescent compound **10**, compared to unstained conditions without compound **10** or with irrelevant isotype control for NRP-1 staining.

Usually, in the presence of its natural ligand, a transmembrane receptor at the cell surface may induce signaling, internalization of complex and recycling at the cell surface. In contrast, some drugs, e.g., blocking antibodies, may induce internalization of antibody-receptor complex and receptor recycling or internalization with an intracellular sequestration, as we previously showed in anti-human transferrin receptor (anti-Tfr) therapy development [92]. Thus, to identify the mechanism of action of the hybrid **10** on the NRP-1 expression on cells, we followed its expression after a time course exposure of cells at 37 °C. Independently of time exposure, the results prove the presence of compound **10** bound with cells (positive from 5/6-FAM-labeled peptide) with no downmodulation of NRP-1 expression (Figure 7a), as we observed strong signal from the stained receptor at each time interval. This might suggest the incapacity of hybrid **10** to induced downmodulation of NRP-1 by cells or its internalization, since only NRP-1 cell surface expression was followed. This intriguing result focused our attention on tracking the level of expression intensity of NRP-1 on the surfaced of MDA-MB-231 cells exposed on compound **10**. Surprisingly, the NRP-1 level expression, in a time-dependent manner, was rapidly increased at the cell surface. The median fluorescent intensity after 1 h (T60) of cell exposure on hybrid 10 was 1.5-fold higher than after 5 min of incubation (Figure 7b). This upregulation of NRP-1 expression could not be explained by a neo-synthesis of NRP-1 from mRNA, which requires more time, but only by the induction of endogenous stock trafficking of intracytoplasmic NRP-1 reserve toward the cell surface. This hypothesis is strengthened here, since MDA-MB-231 expressed a large amount of NRP-1 at the cell surface, but also had plenty of the cytoplasmic counterpart, reaching a maximum of median fluorescence intensity higher than the restricted level of NRP-1 expression at the surface (Figure 7c).

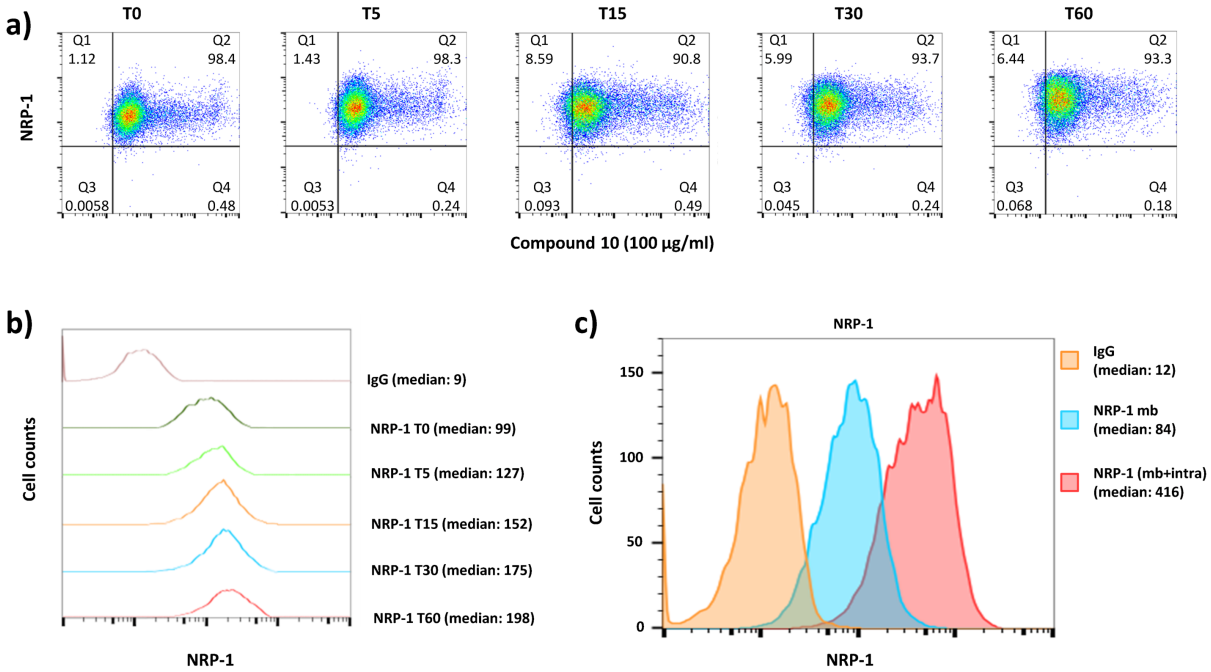

Figure 7. Urea–peptide hybrid **10** modify NRP-1 level expression on MDA-MB-231 breast cancer cells. (**a**) Dot plots show the percentages of NRP-1-positive cells that bind the fluorescent peptide during 37 °C exposure at different times (T = 0 to T = 60 min). (**b**) The histogram shows the NRP-1 level expression modification on cells exposed to compound **10** (100 µg/mL) after 60 (red), 30 (blue), 15 (orange) and 5 (green) min at 37 °C compared to level expression at 4 °C (dark green) and to irrelevant control IgG staining (pink). Median fluorescence intensities of NRP-1 staining are shown for each condition. (**c**) The level expression of NRP-1 at the cell membrane (mb, blue histogram) is overlain on the membrane and intracytoplasmic NRP-1 expression (mb + intra, red histogram), and compared to the irrelevant IgG isotype staining (orange histogram). Median fluorescence intensity of NRP-1 staining is indicated for each histogram.

We believe there are two possibilities that could explain this phenomenon. One is that hybrid/NRP-1 complex is rapidly internalized into the cell and leads to deprivation of NRP-1 on the cell surface, which is followed by induced NRP-1 transport to the cell membrane. Another one is that inhibition of VEGF-A_{165}/NRP-1 complex formation is blocked on the cell surface by hybrid, which causes VEGF-A_{165} deprivation of cells (cells are unable to bind VEGF-A_{165} ligand) and induces rapid NRP-1 stock trafficking to restore VEGF-A_{165} signaling pathways. In both cases, the lack of biochemical signaling is compensated by swift mobilization of NRP-1 intracellular counterpart stock. The process of externalization of an intracellular vesicular pool of receptors was previously observed for other receptors [93].

3. Materials and Methods

3.1. Materials

Unless otherwise specified, reagents were obtained from commercial sources. LC-MS grade water was purchased from Huberlab (Aesch, Switzerland); methanol and acetonitrile (both HPLC gradient grade) were purchased from VWR (Darmstadt, Germany). Ammonium formate and formic acid were purchased from Sigma-Aldrich (Buchs, Switzerland). Other solvents and reagents were purchased from Merck (Darmstadt, Germany). Fmoc-Arg(Pbf) Wang resin was obtained from Activotec (Cambridge, UK). Amino acids and coupling reagents were purchased from Iris Biotech (Marktredwitz, Germany). Recombinant human receptors and biotinylated human VEGF-A_{165} were purchased from R&D Systems (Minneapolis, MN, USA). Chemiluminescent, streptavidin-horseradish peroxidase conjugate and DPBS were obtained from Thermo Scientific (Waltham, MA, USA).

3.2. Succinimidyl Carbamate Building Blocks Synthesis

Activated monomers were prepared using a previously described procedure [75]. Detailed NMR and HRMS data can be found in Supplementary Materials (Figures S1–S5).

Urea–peptide hybrids' synthesis. Synthesis of urea–peptide hybrids was done manually on the pre-loaded Fmoc-Arg(Pbf) Wang resin with capacity 0.32 mmol/g (0.3 g) following the standard Fmoc chemistry. Coupling of 2 eq protected amino acids (0.19 mmol) was done using 2 eq HCTU (79 mg, 0.19 mmol) and 5 eq DIPEA (81 µL, 0.48 mmol) in DMF (3 mL). For the deprotection step, 20% piperidine in DMF was used. Coupling of protected succinimidyl carbamate building blocks was done following previously reported procedures [75]: 1.5 eq of building block (0.14 mmole) was dissolved in 3 mL of DMF with the addition of 2.5 eq of DIPEA (41 µL, 0.24 mmol). The synthesis was supported by microwave irradiation (60 °C, 50 W, 2 × 15 min). The resin was filtered and washed with DMF (4 × 3 mL). The reduction of azide group was performed with 1M Pme_3 solution in THF (10 eq relative to the resin loading) in a mixture of 1,4-dioxane:H_2O (3 mL, 7:3, *v*:*v*) under the microwave irradiation (60 °C, 50 W, 2 × 30 min). After the reaction, the resin was filtered and washed with 1,4-dioxane:H_2O (1 × 3 mL) and DMF (4 × 3 mL). Guanidinylation reaction was carried out using 5 eq of 3,5-dimethylpyrazole-1-carboxamidine nitrate (DMPCN, 96 mg, 0.48 mmol) dissolved in 3 mL of DMF with 19.5 eq of DIPEA (320 µL, 1.9 mmol) for 7 days. 5/6-FAM was coupled using the same equivalents of reagents for amino acids, but reaction was carried out overnight in darkness.

After the synthesis, the resin was dried and final compounds were cleaved from the resin using 5 mL TFA:H_2O:TIS (95:2.5:2.5, *v*:*v*:*v*) for 3 h and then precipitated by dropwise addition into a cold Et_2O. Crude peptides were collected by centrifugation and purified by preparative RP-HPLC (Duisburg, Germany) on a C12 column (Torrance, CA, USA) with H_2O/ACN gradient containing 0.1% TFA. Pure compounds were analyzed with the Shimadzu Prominence analytical HPLC system (Duisburg, Germany). Molecular weight and elemental composition were confirmed using a TripleTOF 6600 mass spectrometer (Sciex, Concord, Ontario, Canada). Detailed RP-HPLC, HRMS and MS/MS data can be found in Supplementary Materials (Figures S6–S15).

3.3. Competitive Receptor Binding Assays

This method was previously described for NRP-1 [44–46]. Briefly, overnight coating at 4 °C of the flat bottom surface of a 96-well plate with 100 µL (200 ng/well) recombinant human NRP-1, NRP-2, VEGFR-1 or VEGFR-2 was followed by non-specific interactions blocking using 0.5% bovine serum albumin (BSA) in PBS. Next, 50 µL of urea–peptide hybrid in PBS and 50 µL (400 ng/mL) of human (bt)-VEGF-A_{165} in PBS containing 4 µg/mL of heparin were added respectively. Plates were incubated for 2 h at RT, and then washed and treated with streptavidin-horseradish peroxidase conjugate in PBS (1:8000). Next, 100 µL chemiluminescent substrate was added, and luminescence was quantified using Tecan Infinite F200Pro microplate reader (Männedorf, Switzerland). In a positive control (P) only (bt)-VEGF-A_{165} was present in wells. Not coated by receptor wells were treated as a negative control (N). Percentages of inhibition were calculated by the following formula:

$$100\% - [[(S - N)/(P - N)] \cdot 100\%] \quad (1)$$

where S is the signal intensity measured in wells with urea–peptide hybrid. The IC_{50} of each urea–peptide hybrid was calculated using the nonlinear regression function with GraphPad Prism Version-5.01 (GraphPad Software, San Diego, CA, USA). Data are presented as log (inhibitor) versus normalized response-variable slope (Figure S16). Data are the means ± SEMs of two or three independent experiments, each performed in triplicate.

3.4. 2D NMR Spectroscopy

2D NMR spectra of parent peptide and hybrid **6** were recorded on Agilent DD2 600 MHz spectrometer. The compounds were dissolved in 9:1 DPBS buffer:D_2O at a

concentration of around 10 mg/mL. 1D spectra were recorded with a double pulsed field gradient spin echo (DPFGSE) water signal suppression sequence. Sequences and parameters for 2D spectra were as follows: TOCSY DPFGSE water signal suppression—512 × 256 time domain complex points zero-filled to 2048 × 1024 complex points, and apodized by cosine square function in both dimensions; spectral width 6 kHz in both dimensions; number of scans 16 and mixing time 65 ms. ROESY DPFGSE water signal suppression—512 × 256 time domain complex points zero-filled to 2048 × 1024 complex points, and apodized by cosine square function in both dimensions; spectral width 6 kHz in both dimensions; number of scans 48 and mixing time 200 ms. 13C-1H HSQC—1442 × 400 time domain complex points zero-filled to 2048 × 1024 complex points, and apodized by cosine square function in both dimensions; spectral width 9.6 × 25.6 kHz in F2 and F1, respectively; number of was scans 8. COSY water signal suppression using presaturation—900 × 256 time domain complex points zero-filled to 2048 × 2048 complex points, and apodized by cosine square function on both dimensions; spectral width 6 kHz in both dimensions; number of scans 16.

3.5. Molecular Dynamic Studies

Ligand–protein interactions were studied by molecular dynamics (MD) in GROMACS 2018.2 [94]. Input structures were prepared by superposing C-terminal Arg part of studied compounds, on the C-terminal Arg of tuftsin (TKPR) found in 2ORZ crystallographic structure of NRP-1 tuftsin complex. CHARMM-GUI service [95] was used to solvate the complexes (rectangular waterbox, TIP3 waters, almost 48,000 water molecules). In total, 0.154 M of Na^+ and Cl^- ions was added to neutralize the system. The protonation states in ligands and in the protein were set as assumed in pH 7. CHARMM36 force field was used [96]. Unnatural amino acids topologies and parameters were compiled either from existing CHARMM36 values or taken from SwissSideChain [97]. The systems were subject to minimization and NVT equilibration. The production step (NPT ensemble, T $\frac{1}{4}$ 303.15 K, integration step $\frac{1}{4}$ 2 fs, cut-off scheme Verlet, Nose-Hoover thermostat, Parrinello-Rahman barostat, LINCS H-bonds constraints) followed. The production lasted 200 ns and was repeated six times (each time from the same starting point) giving 1200 ns for every compound in total. Analysis and visualization of results were performed in Gromacs and UCSF Chimera [98].

3.6. Blood Collection and Serum Preparation

The study was conducted in full accordance with ethical principles in accordance with the ICH E6 (R2) Guideline for Good Clinical Practice and the Code of Good Customs in Science developed by the Polish Academy of Sciences. Signed consent for using serum was obtained from volunteers. The Rector's Commission for Ethics of Scientific Research with Human Participation, University of Warsaw, Warsaw, Poland gave the ethical approval (approval number 51/2020). Human blood from four healthy persons was directly drawn into evacuated tubes and left undisturbed at room temperature for 1 h to clot. Tubes were centrifuged at 2500× *g* for 10 min to prevent possible platelet activation. Serum was pipetted out of the blood collection tubes, pooled and collected in microtubes.

3.7. In Vitro Enzymatic Stability Assay

A degradation assay was adapted from a method described previously [42,44–46]. Human blood serum was preactivated in Eppendorf ThermoMixer® Comfort (Hamburg, Germany) at 37 °C for 20 min (350 rpm). Next, 20 µL of aqueous urea–peptide hybrid stock solution was added to give ~750 µg/mL final compound concentration, and incubation was continued. At selected time intervals, 50 µL of the mixture was collected and quenched by adding 200 µL of ACN:H_2O:FA mixture (89:10:1, *v*:*v*:*v*). The obtained suspension was vortexed for 1 min (3000 min^{-1}) and centrifuged for 10 min in 4 °C (11,000× *g*). 100 µL of supernatant was collected and lyophilized. The samples reconstituted in 1 mL of 10 mM ammonium formate with 0.1% FA were subjected to LC-MS. Relative concentration at time

intervals was calculated using peak area of either individual or most intense fragment of compound of interest. Analyst software version 1.7.1 was used for data acquisition, Peak View 2.2 and MultiQuant 2.1 (Sciex, ON) were used for data processing. Detailed analytical data can be found in Supplementary Materials (Figures S17–S45). GraphPad Prism Version-5.01 was used to present data and statistics. All experiments were independently conducted three times and results are represented as means ± SEMs. In order to show the significant difference in the concentration of intact substrate at each time interval depending on the sequence of the hybrid, a two-way ANOVA with Bonferroni's post-tests was done (** $p < 0.01$, *** $p < 0.001$).

3.8. Cell Culture

The breast cancer cell line MDA-MB-231 was purchased from ATCC (France) and cultured in presence of DMEM complemented with 10% fetal calf serum (FCS), 1% penicillin–streptomycin and 1% glutamine (Invitrogen, France) at 37 °C, 5% CO_2.

3.9. Flow Cytometry Analysis of Membrane and Intracytoplasmic NRP-1 Expression

Cells were harvested using a mix of EDTA/Trypsin buffer (Invitrogen, France) to detach cells from plastic after 5 min exposure at 37 °C. Then cells were washed twice with complete medium to inactivate trypsin. Cell pellet was washed with 1X PBS with 2% FCS to perform FACS analysis. Cells were stained for 15 min at 4 °C with anti-neuropilin monoclonal antibodies BDCA-4: AD5-17F6 clone (Miltenyi Biotec®, France) or 12C2 clone (BioLegend®, USA), and with appropriate irrelevant IgG as control, both labeled with –PE or –APC, respectively. Intracytoplasmic staining was performed on 15 min PFA 4% fixed cells which were then permeabilized and stained using Saponin 2× buffer with antibodies described above. After washing with PBS containing 2% FCS, stained cells were analyzed using BD FACSCalibur™ (San Jose, CA, USA) and FlowJo™ cell analysis software (FlowJo LLC, Ashland, OR, USA).

3.10. Labelled Urea–Peptide Hybrid Binding Assays at 4 °C

Harvested cells were plated in 1× PBS, 2% FCS buffer in the absence or presence of 5/6-FAM-hybrid (**10**) at several concentrations (100, 50, 25 and 12.5 µg/mL) during 15 min at 4 °C. Unstained and FITC-irrelevant IgG cells were used as controls. Then, cells were washed with 1× PBS, 2% FCS buffer before BD FACSCalibur™ acquisition and FlowJo™ software analysis. This binding experiment is associated with a sequential NRP-1 staining (using clones describes above) or with appropriate irrelevant IgG as control (15 min at 4 °C) when it is necessary to prove the lack of antigen competition access for antibodies.

3.11. Labelled Urea–Peptide Hybrid Binding Assays at 37 °C

Cells were stained with 5/6-FAM labeled urea–peptide hybrid (**10**) (100 µg/mL) at 4 °C, as described above. Next, washed cells were sequentially incubated at 37 °C during 0, 5, 15, 30 and 60 min in complete culture medium. After an ultimate wash with PBS supplemented with 2% FCS, cells were stained with APC-NRP-1 antibody or APC-irrelevant IgG as a control (15 min at 4°C). BD FACSCaliburTM acquisition and FlowJoTM software analysis were then performed.

4. Conclusions

In this work, we presented a new group of urea–peptide hybrids based on our previous active structure Lys (*h*Arg)-Dab-Oic-Arg with improved inhibition of $VEGF_{165}$/NRP-1 complex formation. The aim of our SAR study was to optimize the urea unit position in the branched portion of the parent molecule, which is important for ligand–protein interactions, and at the same time is a major enzyme cleavage site. The obtained results indicate that one of the synthesized compounds, namely, the hybrid **6** with the substitution of the Lys (*h*Arg) fragment by the containing urea bond fragment Dab($hArg^U$), compared to the parent compound, showed not only an increase in the affinity for NRP-1 12-fold, but also a

significant decrease in enzymatic degradation, by eliminating enzymatic cleavage of the branching. The latter feature is very important, as the prolongation of the plasma half-life is one of the crucial parameters of prospective drugs, as it helps to extend the time between drug applications. While the performed molecular dynamic and 2D NMR experiments did not give a direct answer for the increase in affinity due to unstable conformations of the analyzed compounds, the data suggest that urea moiety may favor additional ligand–protein interactions. Moreover, the presented in vitro experiments allowed us to prove that 5/6-FAM-labeled compound **6** binds to NRP-1 on the cell membrane and very quickly induces intracytoplasmic NRP-1 stock trafficking to the cell surface. In the near future, we plan to examine the signal paths that accompany this phenomenon. In summary, all the above-mentioned properties make hybrid **6** a good candidate for further development as an inhibitor of $VEGF_{165}$/NRP-1 interaction.

Supplementary Materials: Supplementary materials can be found at https://www.mdpi.com/1422-0067/22/1/72/s1.

Author Contributions: Conceptualization, A.K.P. and A.M.; methodology, A.K.P., P.S. and Y.L.; formal analysis, A.K.P., P.S., K.P.-Z., R.R.-B. and Y.L.; investigation, A.K.P., P.S. and Y.L.; writing—original draft preparation, A.K.P. and P.S.; writing—review and editing, A.M., Y.L., K.P.-Z., R.R.-B., O.H., and G.H.; supervision, A.K.P.; project administration, A.K.P.; funding acquisition, A.K.P. and A.M. All authors have read and agreed to the published version of the manuscript.

Funding: This research was funded by Narodowe Centrum Nauki (National Science Centre, Poland), grant numbers 2017/27/N/NZ7/02473 and 2019/33/B/NZ7/02818. Campus France and French Embassy in Warsaw financially supported A.K.P. under the scholarship number 964117C.

Acknowledgments: The computations were performed at University of Geneva on the Baobab cluster. A.K.P. thanks the Scientific Centre in Paris, Polish Academy of Science, for help in organizing stays in Paris.

Conflicts of Interest: The authors declare no conflict of interest.

Abbreviations

anti-Tfr	anti-human transferrin receptor
5/6-FAM	5/6-carboxyfluorescein
Boc	tert-butoxycarbonyl
BSA	bovine serum albumin
bt	linear dichroism
Dab	2,4-diaminobutyric acid
Dap	2,3-diaminopropionic acid
DIPEA	*N*,*N*-diisopropylethylamine
ELISA	enzyme-linked immunosorbent assay
FACS	fluorescence-activated cell sorting
FCS	foetal calf serum
Fmoc	9-fluorenylmethoxycarbonyl
*h*Arg	homoarginine
HCTU	O-(1*H*-6-chlorobenzotriazole-1-yl)-1,1,3,3-tetramethyluronium hexafluorophosphate
NRP	neuropilin
Oic	octahydroindole-2-carboxylic acid
PBS	phosphate buffer saline
SAR	structure–activity relationship
strep-HRP	streptavidin–horseradish peroxidase conjugate
SWATH	sequential window acquisition of all theoretical mass spectra
TIS	triisopropylsilane
TFA	trifluoroacetic acid
VEGF	vascular endothelial grow factor

References

1. Ferrara, N. Role of vascular endothelial growth factor in regulation of physiological angiogenesis. *Am. J. Physiol. Cell Physiol.* **2001**, *280*, C1358–C1366. [CrossRef] [PubMed]
2. Hicklin, D.J.; Ellis, L.M. Role of the Vascular Endothelial Growth Factor Pathway in Tumor Growth and Angiogenesis. *J. Clin. Oncol.* **2005**, *23*, 1011–1027. [CrossRef] [PubMed]
3. Waltenberger, J.; Claesson-Welsh, L.; Siegbahn, A.; Shibuya, M.; Heldin, C.H. Different signal transduction properties of KDR and Flt1, two receptors for vascular endothelial growth factor. *J. Biol. Chem.* **1994**, *269*, 26988–26995. [PubMed]
4. Ferrara, N.; Gerber, H.-P.; LeCouter, J. The biology of VEGF and its receptors. *Nat. Med.* **2003**, *9*, 669–676. [CrossRef]
5. Bergantino, F.; Guariniello, S.; Raucci, R.; Colonna, G.; De Luca, A.; Normanno, N.; Costantini, S. Structure–fluctuation–function relationships of seven pro-angiogenic isoforms of VEGFA, important mediators of tumorigenesis. *Biochim. Biophys. Acta* **2015**, *1854*, 410–425. [CrossRef]
6. Soker, S.; Takashima, S.; Miao, H.Q.; Neufeld, G.; Klagsbrun, M. Neuropilin-1 Is Expressed by Endothelial and Tumor Cells as an Isoform-Specific Receptor for Vascular Endothelial Growth Factor. *Cell* **1998**, *92*, 735–745. [CrossRef]
7. Carmeliet, P. Angiogenesis in life, disease and medicine. *Nature* **2005**, *438*, 932–936. [CrossRef]
8. Koch, S. Neuropilin signalling in angiogenesis. *Biochem. Soc. Trans.* **2012**, *40*, 20–25. [CrossRef]
9. Djordjevic, S.; Driscoll, P.C. Targeting VEGF signalling via the neuropilin co-receptor. *Drug Discov. Today* **2013**, *18*, 447–455. [CrossRef]
10. Neufeld, G.; Cohen, T.; Shraga, N.; Lange, T.; Kessler, O.; Herzog, Y. The Neuropilins: Multifunctional Semaphorin and VEGF Receptors that Modulate Axon Guidance and Angiogenesis. *Trends Cardiovasc. Med.* **2002**, *12*, 13–19. [CrossRef]
11. Roy, S.; Bag, A.K.; Singh, R.K.; Talmadge, J.E.; Batra, S.K.; Datta, K. Multifaceted Role of Neuropilins in the Immune System: Potential Targets for Immunotherapy. *Front. Immunol.* **2017**, *8*, 1228. [CrossRef] [PubMed]
12. Tordjman, R.; Lepelletier, Y.; Lemarchandel, V.; Cambot, M.; Gaulard, P.; Hermine, O.; Roméo, P.-H. A neuronal receptor, neuropilin-1, is essential for the initiation of the primary immune response. *Nat. Immunol.* **2002**, *3*, 477–482. [CrossRef] [PubMed]
13. Latil, A.; Bièche, I.; Pesche, S.; Valéri, A.; Fournier, G.; Cussenot, O.; Lidereau, R. VEGF overexpression in clinically localized prostate tumors and neuropilin-1 overexpression in metastatic forms. *Int. J. Cancer* **2000**, *89*, 167–171. [CrossRef]
14. Stephenson, J.M.; Banerjee, S.; Saxena, N.K.; Cherian, R.; Banerjee, S.K. Neuropilin-1 is differentially expressed in myoepithelial cells and vascular smooth muscle cells in preneoplastic and neoplastic human breast: A possible marker for the progression of breast cancer. *Int. J. Cancer* **2002**, *101*, 409–414. [CrossRef]
15. Parikh, A.A.; Liu, W.B.; Fan, F.; Stoeltzing, O.; Reinmuth, N.; Bruns, C.J.; Bucana, C.D.; Evans, D.B.; Ellis, L.M. Expression and regulation of the novel vascular endothelial growth factor receptor neuropilin-1 by epidermal growth factor in human pancreatic carcinoma. *Cancer* **2003**, *98*, 720–729. [CrossRef]
16. Parikh, A.A.; Fan, F.; Liu, W.B.; Ahmad, S.A.; Stoeltzing, O.; Reinmuth, N.; Bielenberg, D.; Bucana, C.D.; Klagsbrun, M.; Ellis, L.M. Neuropilin-1 in Human Colon Cancer: Expression, Regulation, and Role in Induction of Angiogenesis. *Am. J. Pathol.* **2004**, *164*, 2139–2151. [CrossRef]
17. Folkman, J. Tumor Angiogenesis: Therapeutic Implications. *N. Engl. J. Med.* **1971**, *285*, 1182–1186. [CrossRef]
18. Ausprunk, D.H.; Folkman, J. Migration and proliferation of endothelial cells in preformed and newly formed blood vessels during tumor angiogenesis. *Microvasc. Res.* **1977**, *14*, 53–65. [CrossRef]
19. Grandclement, C.; Borg, C. Neuropilins: A New Target for Cancer Therapy. *Cancers* **2011**, *3*, 1899–1928. [CrossRef]
20. Simons, M.; Ware, J.A. Therapeutic angiogenesis in cardiovascular disease. *Nat. Rev. Drug Discov.* **2003**, *2*, 863–872. [CrossRef]
21. Marina, Z.; Sandra, D.; Lucia, M. Development of New Drugs in Angiogenesis. *Curr. Drug Targets* **2004**, *5*, 485–493. [CrossRef]
22. Jarvis, A.; Allerston, C.K.; Jia, H.; Herzog, B.; Garza-Garcia, A.; Winfield, N.; Ellard, K.; Aqil, R.; Lynch, R.; Chapman, C.; et al. Small Molecule Inhibitors of the Neuropilin-1 Vascular Endothelial Growth Factor A (VEGF-A) Interaction. *J. Med. Chem.* **2010**, *53*, 2215–2226. [CrossRef] [PubMed]
23. Novoa, A.; Pellegrini-Moïse, N.; Bechet, D.; Barberi-Heyob, M.; Chapleur, Y. Sugar-based peptidomimetics as potential inhibitors of the vascular endothelium growth factor binding to neuropilin-1. *Biorg. Med. Chem.* **2010**, *18*, 3285–3298. [CrossRef] [PubMed]
24. Borriello, L.; Montès, M.; Lepelletier, Y.; Leforban, B.; Liu, W.-Q.; Demange, L.; Delhomme, B.; Pavoni, S.; Jarray, R.; Boucher, J.L.; et al. Structure-based discovery of a small non-peptidic Neuropilins antagonist exerting in vitro and in vivo anti-tumor activity on breast cancer model. *Cancer Lett.* **2014**, *349*, 120–127. [CrossRef] [PubMed]
25. Starzec, A.; Miteva, M.A.; Ladam, P.; Villoutreix, B.O.; Perret, G.Y. Discovery of novel inhibitors of vascular endothelial growth factor-A–Neuropilin-1 interaction by structure-based virtual screening. *Biorg. Med. Chem.* **2014**, *22*, 4042–4048. [CrossRef] [PubMed]
26. Liu, W.-Q.; Megale, V.; Borriello, L.; Leforban, B.; Montès, M.; Goldwaser, E.; Gresh, N.; Piquemal, J.-P.; Hadj-Slimane, R.; Hermine, O.; et al. Synthesis and structure–activity relationship of non-peptidic antagonists of neuropilin-1 receptor. *Bioorg. Med. Chem. Lett.* **2014**, *24*, 4254–4259. [CrossRef]
27. Liu, W.-Q.; Lepelletier, Y.; Montès, M.; Borriello, L.; Jarray, R.; Grépin, R.; Leforban, B.; Loukaci, A.; Benhida, R.; Hermine, O.; et al. NRPa-308, a new neuropilin-1 antagonist, exerts in vitro anti-angiogenic and anti-proliferative effects and in vivo anti-cancer effects in a mouse xenograft model. *Cancer Lett.* **2018**, *414*, 88–98. [CrossRef]

28. Powell, J.; Mota, F.; Steadman, D.; Soudy, C.; Miyauchi, J.T.; Crosby, S.; Jarvis, A.; Reisinger, T.; Winfield, N.; Evans, G.; et al. Small Molecule Neuropilin-1 Antagonists Combine Antiangiogenic and Antitumor Activity with Immune Modulation through Reduction of Transforming Growth Factor Beta (TGFβ) Production in Regulatory T-Cells. *J. Med. Chem.* **2018**, *61*, 4135–4154. [CrossRef]
29. Brachet, E.; Dumond, A.; Liu, W.-Q.; Fabre, M.; Selkti, M.; Raynaud, F.; Hermine, O.; Benhida, R.; Belmont, P.; Garbay, C.; et al. Synthesis, 3D-structure and stability analyses of NRPa-308, a new promising anti-cancer agent. *Bioorg. Med. Chem. Lett.* **2019**, *29*, 126710. [CrossRef]
30. Binétruy-Tournaire, R.; Demangel, C.; Malavaud, B.; Vassy, R.; Rouyre, S.; Kraemer, M.; Plouët, J.; Derbin, C.; Perret, G.; Mazié, J.C. Identification of a peptide blocking vascular endothelial growth factor (VEGF)-mediated angiogenesis. *EMBO J.* **2000**, *19*, 1525–1533. [CrossRef]
31. von Wronski, M.A.; Raju, N.; Pillai, R.; Bogdan, N.J.; Marinelli, E.R.; Nanjappan, P.; Ramalingam, K.; Arunachalam, T.; Eaton, S.; Linder, K.E.; et al. Tuftsin Binds Neuropilin-1 through a Sequence Similar to That Encoded by Exon 8 of Vascular Endothelial Growth Factor. *J. Biol. Chem.* **2006**, *281*, 5702–5710. [CrossRef] [PubMed]
32. Starzec, A.; Vassy, R.; Martin, A.; Lecouvey, M.; Di Benedetto, M.; Crépin, M.; Perret, G.Y. Antiangiogenic and antitumor activities of peptide inhibiting the vascular endothelial growth factor binding to neuropilin-1. *Life Sci.* **2006**, *79*, 2370–2381. [CrossRef] [PubMed]
33. Vander Kooi, C.W.; Jusino, M.A.; Perman, B.; Neau, D.B.; Bellamy, H.D.; Leahy, D.J. Structural basis for ligand and heparin binding to neuropilin B domains. *Proc. Natl. Acad. Sci. USA* **2007**, *104*, 6152. [CrossRef] [PubMed]
34. Starzec, A.; Ladam, P.; Vassy, R.; Badache, S.; Bouchemal, N.; Navaza, A.; du Penhoat, C.H.; Perret, G.Y. Structure–function analysis of the antiangiogenic ATWLPPR peptide inhibiting VEGF165 binding to neuropilin-1 and molecular dynamics simulations of the ATWLPPR/neuropilin-1 complex. *Peptides* **2007**, *28*, 2397–2402. [CrossRef]
35. Teesalu, T.; Sugahara, K.N.; Kotamraju, V.R.; Ruoslahti, E. C-end rule peptides mediate neuropilin-1-dependent cell, vascular, and tissue penetration. *Proc. Natl. Acad. Sci. USA* **2009**, *106*, 16157. [CrossRef]
36. Zanuy, D.; Kotla, R.; Nussinov, R.; Teesalu, T.; Sugahara, K.N.; Alemán, C.; Haspel, N. Sequence dependence of C-end rule peptides in binding and activation of neuropilin-1 receptor. *J. Struct. Biol.* **2013**, *182*, 78–86. [CrossRef]
37. Liu, W.-Q.; Borriello, L.; Allain, B.; Pavoni, S.; Lopez, N.; Hermine, O.; Garbay, C.; Raynaud, F.; Lepelletier, Y.; Demange, L. New Peptides Structurally Related to VEGF-A165 Exon-7 and -8 Encoded Domains Antagonize Its Binding to NRP-1 and VEGF-R1. *Int. J. Pept. Res. Ther.* **2015**, *21*, 117–124. [CrossRef]
38. Richard, M.; Chateau, A.; Jelsch, C.; Didierjean, C.; Manival, X.; Charron, C.; Maigret, B.; Barberi-Heyob, M.; Chapleur, Y.; Boura, C.; et al. Carbohydrate-based peptidomimetics targeting neuropilin-1: Synthesis, molecular docking study and in vitro biological activities. *Biorg. Med. Chem.* **2016**, *24*, 5315–5325. [CrossRef]
39. Tymecka, D.; Lipiński, P.F.J.; Fedorczyk, B.; Puszko, A.; Wileńska, B.; Perret, G.Y.; Misicka, A. Structure-activity relationship study of tetrapeptide inhibitors of the Vascular Endothelial Growth Factor A binding to Neuropilin-1. *Peptides* **2017**, *94*, 25–32. [CrossRef]
40. Kamarulzaman, E.E.; Vanderesse, R.; Gazzali, A.M.; Barberi-Heyob, M.; Boura, C.; Frochot, C.; Shawkataly, O.; Aubry, A.; Wahab, H.A. Molecular modelling, synthesis and biological evaluation of peptide inhibitors as anti-angiogenic agent targeting neuropilin-1 for anticancer application. *J. Biomol. Struct. Dyn.* **2017**, *35*, 26–45. [CrossRef]
41. Fedorczyk, B.; Lipiński, P.F.J.; Tymecka, D.; Puszko, A.K.; Wilenska, B.; Perret, G.Y.; Misicka, A. Conformational latitude—Activity relationship of KPPR tetrapeptide analogues toward their ability to inhibit binding of vascular endothelial growth factor 165 to neuropilin-1. *J. Pept. Sci.* **2017**, *23*, 445–454. [CrossRef] [PubMed]
42. Tymecka, D.; Puszko, A.K.; Lipiński, P.F.J.; Fedorczyk, B.; Wilenska, B.; Sura, K.; Perret, G.Y.; Misicka, A. Branched pentapeptides as potent inhibitors of the vascular endothelial growth factor 165 binding to Neuropilin-1: Design, synthesis and biological activity. *Eur. J. Med. Chem.* **2018**, *158*, 453–462. [CrossRef] [PubMed]
43. Fedorczyk, B.; Lipiński, P.F.J.; Puszko, A.K.; Tymecka, D.; Wilenska, B.; Dudka, W.; Perret, G.Y.; Wieczorek, R.; Misicka, A. Triazolopeptides Inhibiting the Interaction between Neuropilin-1 and Vascular Endothelial Growth Factor-165. *Molecules* **2019**, *24*, 1756. [CrossRef] [PubMed]
44. Puszko, A.K.; Sosnowski, P.; Tymecka, D.; Raynaud, F.; Hermine, O.; Lepelletier, Y.; Misicka, A. Neuropilin-1 peptide-like ligands with proline mimetics, tested using the improved chemiluminescence affinity detection method. *MedChemComm* **2019**, *10*, 332–340. [CrossRef]
45. Puszko, A.K.; Sosnowski, P.; Pułka-Ziach, K.; Hermine, O.; Hopfgartner, G.; Lepelletier, Y.; Misicka, A. Urea moiety as amide bond mimetic in peptide-like inhibitors of VEGF-A165/NRP-1 complex. *Bioorg. Med. Chem. Lett.* **2019**, *29*, 2493–2497. [CrossRef]
46. Puszko, A.K.; Sosnowski, P.; Raynaud, F.; Hermine, O.; Hopfgartner, G.; Lepelletier, Y.; Misicka, A. Does Cysteine Rule (CysR) Complete the CendR Principle? Increase in Affinity of Peptide Ligands for NRP-1 Through the Presence of N-Terminal Cysteine. *Biomolecules* **2020**, *10*, 448. [CrossRef]
47. Jia, H.; Bagherzadeh, A.; Hartzoulakis, B.; Jarvis, A.; Löhr, M.; Shaikh, S.; Aqil, R.; Cheng, L.; Tickner, M.; Esposito, D.; et al. Characterization of a Bicyclic Peptide Neuropilin-1 (NP-1) Antagonist (EG3287) Reveals Importance of Vascular Endothelial Growth Factor Exon 8 for NP-1 Binding and Role of NP-1 in KDR Signaling. *J. Biol. Chem.* **2006**, *281*, 13493–13502. [CrossRef]

48. Jia, H.; Aqil, R.; Cheng, L.; Chapman, C.; Shaikh, S.; Jarvis, A.; Chan, A.W.E.; Hartzoulakis, B.; Evans, I.M.; Frolov, A.; et al. N-Terminal Modification of VEGF-A C Terminus-Derived Peptides Delineates Structural Features Involved in Neuropilin-1 Binding and Functional Activity. *ChemBioChem* **2014**, *15*, 1161–1170. [CrossRef]
49. Grabowska, K.; Puszko, A.K.; Lipiński, P.F.J.; Laskowska, A.K.; Wileńska, B.; Witkowska, E.; Misicka, A. Design, synthesis and in vitro biological evaluation of a small cyclic peptide as inhibitor of vascular endothelial growth factor binding to neuropilin-1. *Bioorg. Med. Chem. Lett.* **2016**, *26*, 2843–2846. [CrossRef]
50. Grabowska, K.; Puszko, A.K.; Lipiński, P.F.J.; Laskowska, A.K.; Wileńska, B.; Witkowska, E.; Perret, G.Y.; Misicka, A. Structure-activity relationship study of a small cyclic peptide H-c[Lys-Pro-Glu]-Arg-OH: A potent inhibitor of Vascular Endothelial Growth Factor interaction with Neuropilin-1. *Biorg. Med. Chem.* **2017**, *25*, 597–602. [CrossRef]
51. Lau, J.L.; Dunn, M.K. Therapeutic peptides: Historical perspectives, current development trends, and future directions. *Biorg. Med. Chem.* **2018**, *26*, 2700–2707. [CrossRef] [PubMed]
52. Parker, M.W.; Xu, P.; Li, X.; Vander Kooi, C.W. Structural Basis for Selective Vascular Endothelial Growth Factor-A (VEGF-A) Binding to Neuropilin-1. *J. Biol. Chem.* **2012**, *287*, 11082–11089. [CrossRef]
53. Keyt, B.A.; Berleau, L.T.; Nguyen, H.V.; Chen, H.; Heinsohn, H.; Vandlen, R.; Ferrara, N. The Carboxyl-terminal Domain(111165) of Vascular Endothelial Growth Factor Is Critical for Its Mitogenic Potency. *J. Biol. Chem.* **1996**, *271*, 7788–7795. [CrossRef] [PubMed]
54. Soker, S.; Gollamudi-Payne, S.; Fidder, H.; Charmahelli, H.; Klagsbrun, M. Inhibition of Vascular Endothelial Growth Factor (VEGF)-induced Endothelial Cell Proliferation by a Peptide Corresponding to the Exon 7-Encoded Domain of VEGF165. *J. Biol. Chem.* **1997**, *272*, 31582–31588. [CrossRef] [PubMed]
55. Fairbrother, W.J.; Champe, M.A.; Christinger, H.W.; Keyt, B.A.; Starovasnik, M.A. Solution structure of the heparin-binding domain of vascular endothelial growth factor. *Structure* **1998**, *6*, 637–648. [CrossRef]
56. Perret, G.Y.; Starzec, A.; Hauet, N.; Vergote, J.; Le Pecheur, M.; Vassy, R.; Léger, G.; Verbeke, K.A.; Bormans, G.; Nicolas, P.; et al. In vitro evaluation and biodistribution of a 99mTc-labeled anti-VEGF peptide targeting neuropilin-1. *Nucl. Med. Biol.* **2004**, *31*, 575–581. [CrossRef]
57. Sugahara, K.N.; Teesalu, T.; Karmali, P.P.; Kotamraju, V.R.; Agemy, L.; Girard, O.M.; Hanahan, D.; Mattrey, R.F.; Ruoslahti, E. Tissue-Penetrating Delivery of Compounds and Nanoparticles into Tumors. *Cancer Cell* **2009**, *16*, 510–520. [CrossRef]
58. Pernot, M.; Vanderesse, R.; Frochot, C.; Guillemin, F.; Barberi-Heyob, M. Stability of peptides and therapeutic success in cancer. *Expert Opin. Drug Metab. Toxicol.* **2011**, *7*, 793–802. [CrossRef]
59. Fosgerau, K.; Hoffmann, T. Peptide therapeutics: Current status and future directions. *Drug Discov. Today* **2015**, *20*, 122–128. [CrossRef]
60. Iguchi, S.; Kawasaki, K.; Okamoto, H.; Umezawa, C.; Okada, Y. Synthesis of Some Pseudo-Peptide Analogs of Thiol Proteinase Inhibitors. *Chem. Pharm. Bull. (Tokyo)* **1999**, *47*, 423–427. [CrossRef]
61. Thomas, N.; Pernot, M.; Vanderesse, R.; Becuwe, P.; Kamarulzaman, E.; Da Silva, D.; François, A.; Frochot, C.; Guillemin, F.; Barberi-Heyob, M. Photodynamic therapy targeting neuropilin-1: Interest of pseudopeptides with improved stability properties. *Biochem. Pharmacol.* **2010**, *80*, 226–235. [CrossRef] [PubMed]
62. Yurek-George, A.; Cecil, A.R.L.; Mo, A.H.K.; Wen, S.; Rogers, H.; Habens, F.; Maeda, S.; Yoshida, M.; Packham, G.; Ganesan, A. The First Biologically Active Synthetic Analogues of FK228, the Depsipeptide Histone Deacetylase Inhibitor. *J. Med. Chem.* **2007**, *50*, 5720–5726. [CrossRef] [PubMed]
63. De Zotti, M.; Biondi, B.; Peggion, C.; De Poli, M.; Fathi, H.; Oancea, S.; Toniolo, C.; Formaggio, F. Partial thioamide scan on the lipopeptaibiotic trichogin GA IV. Effects on folding and bioactivity. *Beilstein J. Org. Chem.* **2012**, *8*, 1161–1171. [CrossRef] [PubMed]
64. Jones, W.C.; Nestor, J.J.; Du Vigneaud, V. Synthesis and some pharmacological properties of [1-deamino-9-thioglycine]oxytocin. *J. Am. Chem. Soc.* **1973**, *95*, 5677–5679. [CrossRef] [PubMed]
65. Lankiewicz, L.; Bowers, C.Y.; Reynolds, G.A.; Labroo, V.; Cohen, L.A.; Vonhof, S.; Sirén, A.-L.; Spatola, A.F. Biological activities of thionated thyrotropin-releasing hormone analogs. *Biochem. Biophys. Res. Commun.* **1992**, *184*, 359–366. [CrossRef]
66. Nahrwold, M.; Bogner, T.; Eissler, S.; Verma, S.; Sewald, N. "Clicktophycin-52": A Bioactive Cryptophycin-52 Triazole Analogue. *Org. Lett.* **2010**, *12*, 1064–1067. [CrossRef] [PubMed]
67. Tam, A.; Arnold, U.; Soellner, M.B.; Raines, R.T. Protein Prosthesis: 1,5-Disubstituted[1,2,3]triazoles as cis-Peptide Bond Surrogates. *J. Am. Chem. Soc.* **2007**, *129*, 12670–12671. [CrossRef]
68. Tischler, M.; Nasu, D.; Empting, M.; Schmelz, S.; Heinz, D.W.; Rottmann, P.; Kolmar, H.; Buntkowsky, G.; Tietze, D.; Avrutina, O. Braces for the Peptide Backbone: Insights into Structure–Activity Relationships of Protease Inhibitor Mimics with Locked Amide Conformations. *Angew. Chem. Int. Ed.* **2012**, *51*, 3708–3712. [CrossRef]
69. Fremaux, J.; Venin, C.; Mauran, L.; Zimmer, R.H.; Guichard, G.; Goudreau, S.R. Peptide-oligourea hybrids analogue of GLP-1 with improved action in vivo. *Nat. Commun.* **2019**, *10*, 924. [CrossRef]
70. Kozikowski, A.P.; Nan, F.; Conti, P.; Zhang, J.; Ramadan, E.; Bzdega, T.; Wroblewska, B.; Neale, J.H.; Pshenichkin, S.; Wroblewski, J.T. Design of Remarkably Simple, Yet Potent Urea-Based Inhibitors of Glutamate Carboxypeptidase II (NAALADase). *J. Med. Chem.* **2001**, *44*, 298–301. [CrossRef]

71. Antunes, S.; Corre, J.-P.; Mikaty, G.; Douat, C.; Goossens, P.L.; Guichard, G. Effect of replacing main-chain ureas with thiourea and guanidinium surrogates on the bactericidal activity of membrane active oligourea foldamers. *Biorg. Med. Chem.* **2017**, *25*, 4245–4252. [CrossRef] [PubMed]
72. Claudon, P.; Violette, A.; Lamour, K.; Decossas, M.; Fournel, S.; Heurtault, B.; Godet, J.; Mély, Y.; Jamart-Grégoire, B.; Averlant-Petit, M.-C.; et al. Consequences of Isostructural Main-Chain Modifications for the Design of Antimicrobial Foldamers: Helical Mimics of Host-Defense Peptides Based on a Heterogeneous Amide/Urea Backbone. *Angew. Chem. Int. Ed.* **2010**, *49*, 333–336. [CrossRef] [PubMed]
73. Cudic, P.; Stawikowski, M. Peptidomimetics: Fmoc Solid-Phase Pseudopeptide Synthesis. In *Peptide-Based Drug Design*; Otvos, L., Ed.; Humana Press: Totowa, NJ, USA, 2008; pp. 223–246. [CrossRef]
74. Tamilarasu, N.; Huq, I.; Rana, T.M. Targeting RNA with peptidomimetic oligomers in human cells. *Bioorg. Med. Chem. Lett.* **2001**, *11*, 505–507. [CrossRef]
75. Douat-Casassus, C.; Pulka, K.; Claudon, P.; Guichard, G. Microwave-Enhanced Solid-Phase Synthesis of *N*,*N*′-Linked Aliphatic Oligoureas and Related Hybrids. *Org. Lett.* **2012**, *14*, 3130–3133. [CrossRef] [PubMed]
76. Carpino, L.A.; Han, G.Y. 9-Fluorenylmethoxycarbonyl amino-protecting group. *J. Org. Chem.* **1972**, *37*, 3404–3409. [CrossRef]
77. Hood, C.A.; Fuentes, G.; Patel, H.; Page, K.; Menakuru, M.; Park, J.H. Fast conventional Fmoc solid-phase peptide synthesis with HCTU. *J. Pept. Sci.* **2008**, *14*, 97–101. [CrossRef]
78. Bernatowicz, M.S.; Wu, Y.; Matsueda, G.R. 1H-Pyrazole-1-carboxamidine hydrochloride an attractive reagent for guanylation of amines and its application to peptide synthesis. *J. Org. Chem.* **1992**, *57*, 2497–2502. [CrossRef]
79. Hopkins, A.L.; Mason, J.S.; Overington, J.P. Can we rationally design promiscuous drugs? *Curr. Opin. Struct. Biol.* **2006**, *16*, 127–136. [CrossRef]
80. Huggins, D.J.; Sherman, W.; Tidor, B. Rational Approaches to Improving Selectivity in Drug Design. *J. Med. Chem.* **2012**, *55*, 1424–1444. [CrossRef]
81. Rossignol, M.; Gagnon, M.L.; Klagsbrun, M. Genomic Organization of Human Neuropilin-1 and Neuropilin-2 Genes: Identification and Distribution of Splice Variants and Soluble Isoforms. *Genomics* **2000**, *70*, 211–222. [CrossRef]
82. Pellet-Many, C.; Frankel, P.; Jia, H.; Zachary, I. Neuropilins: Structure, function and role in disease. *Biochem. J.* **2008**, *411*, 211–226. [CrossRef] [PubMed]
83. Guo, H.-F.; Vander Kooi, C.W. Neuropilin Functions as an Essential Cell Surface Receptor. *J. Biol. Chem.* **2015**, *290*, 29120–29126. [CrossRef] [PubMed]
84. Muller, Y.A.; Li, B.; Christinger, H.W.; Wells, J.A.; Cunningham, B.C.; de Vos, A.M. Vascular endothelial growth factor: Crystal structure and functional mapping of the kinase domain receptor binding site. *Proc. Natl. Acad. Sci. USA* **1997**, *94*, 7192. [CrossRef] [PubMed]
85. Peach, C.J.; Mignone, V.W.; Arruda, M.A.; Alcobia, D.C.; Hill, S.J.; Kilpatrick, L.E.; Woolard, J. Molecular Pharmacology of VEGF-A Isoforms: Binding and Signalling at VEGFR2. *Int. J. Mol. Sci.* **2018**, *19*, 1264. [CrossRef]
86. Dyson, H.J.; Wright, P.E. Defining Solution Conformations of Small Linear Peptides. *Annu. Rev. Biophys. Biophys. Chem.* **1991**, *20*, 519–538. [CrossRef]
87. Kontermann, R.E. Half-life extended biotherapeutics. *Expert Opin. Biol. Ther.* **2016**, *16*, 903–915. [CrossRef]
88. Bonner, R.; Hopfgartner, G. SWATH data independent acquisition mass spectrometry for metabolomics. *TrAC Trends Anal. Chem.* **2019**, *120*, 115278. [CrossRef]
89. Raetz, M.; Duchoslav, E.; Bonner, R.; Hopfgartner, G. Hybrid SWATH/MS and HR-SRM/MS acquisition for phospholipidomics using QUAL/QUANT data processing. *Anal. Bioanal. Chem.* **2019**, *411*, 5681–5690. [CrossRef]
90. Cifuentes Girard, M.F.; Ruskic, D.; Böhm, G.; Picenoni, R.; Hopfgartner, G. Automated parallel derivatization of metabolites with SWATH-MS data acquisition for qualitative and quantitative analysis. *Anal. Chim. Acta* **2020**, *1127*, 198–206. [CrossRef]
91. Narazaki, M.; Tosato, G. Ligand-induced internalization selects use of common receptor neuropilin-1 by VEGF165 and semaphorin3A. *Blood* **2006**, *107*, 3892–3901. [CrossRef]
92. Lepelletier, Y.; Camara-Clayette, V.; Jin, H.; Hermant, A.; Coulon, S.; Dussiot, M.; Arcos-Fajardo, M.; Baude, C.; Canionni, D.; Delarue, R.; et al. Prevention of Mantle Lymphoma Tumor Establishment by Routing Transferrin Receptor toward Lysosomal Compartments. *Cancer Res.* **2007**, *67*, 1145. [CrossRef] [PubMed]
93. Maisel, A.S.; Motulsky, H.J.; Insel, P.A. Propranolol treatment externalizes beta-adrenergic receptors in guinea pig myocardium and prevents further externalization by ischemia. *Circ. Res.* **1987**, *60*, 108–112. [CrossRef] [PubMed]
94. Abraham, M.J.; Murtola, T.; Schulz, R.; Páll, S.; Smith, J.C.; Hess, B.; Lindahl, E. GROMACS: High performance molecular simulations through multi-level parallelism from laptops to supercomputers. *SoftwareX* **2015**, *1–2*, 19–25. [CrossRef]
95. Lee, J.; Cheng, X.; Swails, J.M.; Yeom, M.S.; Eastman, P.K.; Lemkul, J.A.; Wei, S.; Buckner, J.; Jeong, J.C.; Qi, Y.; et al. CHARMM-GUI Input Generator for NAMD, GROMACS, AMBER, OpenMM, and CHARMM/OpenMM Simulations Using the CHARMM36 Additive Force Field. *J. Chem. Theory Comput.* **2016**, *12*, 405–413. [CrossRef]
96. Huang, J.; MacKerell Jr, A.D. CHARMM36 all-atom additive protein force field: Validation based on comparison to NMR data. *J. Comput. Chem.* **2013**, *34*, 2135–2145. [CrossRef]

97. Gfeller, D.; Michielin, O.; Zoete, V. SwissSidechain: A molecular and structural database of non-natural sidechains. *Nucleic Acids Res.* **2012**, *41*, D327–D332. [CrossRef]
98. Pettersen, E.F.; Goddard, T.D.; Huang, C.C.; Couch, G.S.; Greenblatt, D.M.; Meng, E.C.; Ferrin, T.E. UCSF Chimera—A visualization system for exploratory research and analysis. *J. Comput. Chem.* **2004**, *25*, 1605–1612. [CrossRef]